Anomalous conditional counting statistics in an electron-spin-resonance quantum dot measured by a quantum point contact

Yi Ding [1,2] Yiying Yan [1] Jing Hu,[1] Georg Engelhardt [3,4,5] and JunYan Luo [1,*]

[1]*Department of Physics, Zhejiang University of Science and Technology, Hangzhou 310023, China*

[2]*Department of Physics, Babeş-Bolyai University, 400084 Cluj-Napoca, Romania*

[3]*Shenzhen Institute for Quantum Science and Engineering, Southern University of Science and Technology, Shenzhen 518055, China*

[4]*International Quantum Academy, Shenzhen 518048, China*

[5]*Guangdong Provincial Key Laboratory of Quantum Science and Engineering, Southern University of Science and Technology, Shenzhen, 518055, China*

(Received 28 September 2023; accepted 1 March 2024; published 18 March 2024)

A detailed understanding of the full measurement statistics in experiments is the basis for thorough device characterization and advanced applications such as quantum metrology. In this spirit, we investigate the conditional counting statistics of an electron-spin-resonance pumped quantum dot (QD), which is tunnel-coupled to a side electrode and continuously monitored by a quantum point contact (QPC). For such a noninvasive detector, we find that the spin current through the QD and its related cumulants exhibit intriguing features and system parameter dependences when conditioned on the QPC current, which are in strong contrast to the unconditional cumulants. By turning the perspective around and considering the counting statistics of the QPC current conditioned on the QD current, we reveal an anomalous conditional QPC current noise, which is surprisingly suppressed for increasing coupling to the environment. Our results show that information backaction can substantially render statistical transport fluctuations. This unique advantage of the conditional counting statistics in probing the underlying correlations between system and detector, even for noninvasive measurements, can thus be employed for improving measurement protocols in quantum metrology.

DOI: 10.1103/PhysRevB.109.115136

I. INTRODUCTION

The essence of quantum measurements is the tradeoff between acquisition of system information and the detection-induced state reduction, which acts as an effective backaction on the state of the system [1–4]. In contrast to a classical measurement which in principle allows for unlimited degree of specific system information, randomness is inevitably involved in quantum measurements, imposing a fundamental limit on the information attainability by the Heisenberg's uncertainty principle [5–8]. An important figure of merit is to deduce system information encoded in the detector and understand how it alters the remaining uncertainty in the quantum system [9,10].

The state-of-the-art nanofabrication technology has enabled on-chip measurement of individual electron transport in an accurate and continuous manner [11–16]. Yet, the charge quantization gives rise to inherent randomness, which can be analyzed systematically based on full counting statistics (FCS) [17,18]. It has been shown that FCS serves actually as a powerful diagnostic tool to unveil unique system information. In a typical single QD transport system, the FCS is infered from the current through a nearby QPC, where the dynamics and output of the QD is unaffected by the QPC measurement on the ensemble average level [19]. In a quantum trajectory associated with a realtime experimental measurement, however, the system state is updated dependent on the measurement outcome during the continuous monitoring by a QPC, leading thus to a conditional (Bayesian) detection backaction. In quantum systems, this information or statistical backaction has both a classical and a quantum contribution: On the one hand, a measurement updates the (classical) knowledge which we have about the system state, leading thus to a modified time evolution. On the other hand, a quantum measurement inevitably leads to state-reduction that destroys coherences in the measurement basis. The information backaction has a central role to play in the informational approach to detection [20–24]. Instead of the unconditional FCS, this information backaction is described by the conditional counting statistics (CCS): The statistical current fluctuations in one system given the observation of a particular current in the other one [25].

Thus far, CCS has been investigated in systems within the description framework of classic rate equations [25,26]. For a typical setup of electron transport through a single QD monitored by a QPC, the conditional backaction on the system gives rise to a number of novel effects in the CCS compared to the unconditional FCS [25]. The presence of a strong Coulomb interaction leads to additional correlations between transferred electron spins, which may serve as a sensitive tool to detect many-body interactions in mesoscopic transport systems [26]. Recently, CCS has been analyzed in

*jyluo@zust.edu.cn

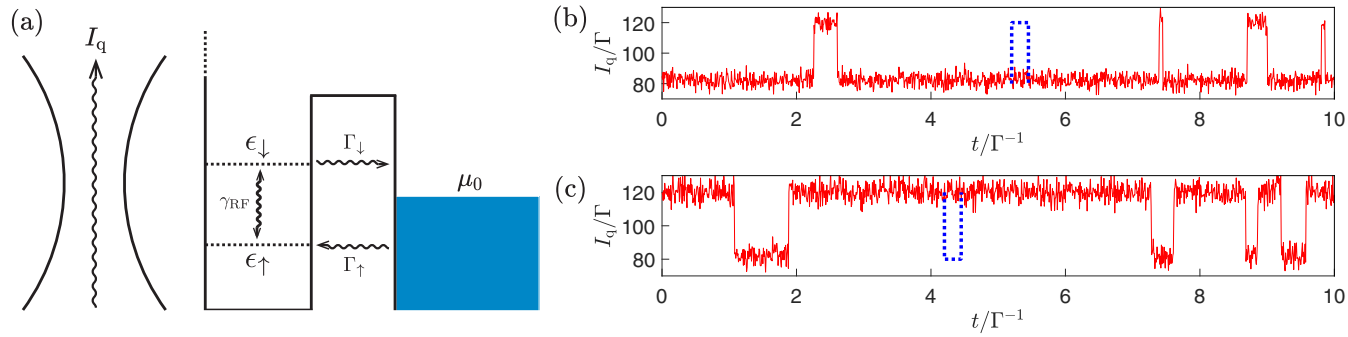

FIG. 1. (a) Schematics of an ESR pumped QD tunnel-coupled to a side electrode, which is continuously monitored by a noninvasive QPC detector. (b) Simulation of the QPC current for $\Gamma_\uparrow = 9\Gamma_\downarrow$ and (c) simulation of the QPC current for $\Gamma_\downarrow = 9\Gamma_\uparrow$, which are obtained using the quantum trajectory method. We set $\Gamma = \Gamma_\uparrow + \Gamma_\downarrow$ as unit of energy and choose $I_0 = 120\Gamma$ and $I_1 = 80\Gamma$.

the quantum regime for transport through a double quantum dot system [27]. For electron transport through a double quantum dot (DQD) measured by a QPC [28], the QPC is modeled as a tunneling junction whose conductance is susceptible to changes in the surrounding electrostatic environment (the occupation configurations of the DQD). The asymmetrical electrostatic coupling between the DQD and the QPC results in different QPC currents, i.e., $I^{\rm L}_{\rm QPC}$ ($I^{\rm R}_{\rm QPC}$) when the left (right) dot of the DQD is occupied. It is due to this mechanism that the QPC is able to distinguish between different charge states in the DQD. This however gives rises to a measurement-induced dephasing of the DQD system $\gamma_{\rm d} = \frac{1}{2}(\sqrt{I^{\rm L}_{\rm QPC}} - \sqrt{I^{\rm R}_{\rm QPC}})^2$ [29,30]. It is therefore appealing to explore the CCS in a quantum system where the quantum coherence is fully retained during the measurement and explore the intimate correlation between system dynamics and the detection process.

This work is dedicated to unveil the underlying correlations by investigating the CCS of an electron-spin-resonance (ESR) system as schematically shown in Fig. 1(a), where the spin-resolved tunneling between the QD and the side electrode is continuously measured by a nearby QPC detector based on a spin-to-charge conversion mechanism [31–35]. The electrostatic coupling between the QD and QPC enables the QPC detector to sense the presence (or absence) of an extra electron on the QD. The Fermi energy of the side electrode is adjusted between the Zeeman sublevels such that only spin-up electrons can tunnel into the QD and spin-down electrons tunnel out at low temperatures. Whenever an extra spin up (down) electron tunnels into (out of) the QD, a down (up) jump takes place in the QPC current as shown in Figs. 1(b) and 1(c). After an electron has tunneled into the QD, it may hop between the $|\uparrow\rangle$ and $|\downarrow\rangle$ spin states, but the QPC will stay in the low-current level as long as the electron remains on the QD. That means the QPC is unable to detect the spin state of the electron, as the QPC can only sense whether the QD is occupied or not, regardless of the spin states. Yet, the QPC is able to detect spin-resolved tunneling without distinguishing between different spin states in the QD and thus does not give rise to any measurement-induced dephasing. We reveal that even for such a noninvasive QPC detector, the measurement leads to a substantial change in the conditional spin-resolved current fluctuations in contrast to the unconditional FCS. In particular, the detector's information backaction gives rise to intriguing spin-resolved conditional statistics and signal-to-noise ratios, which depends sensitively on the magnetic field. We furthermore turn the perspective around and investigate the statistical QPC cumulants conditioned on the spin-resolved current through the QD, where anomalous conditional noise characteristics is observed in regard to its dependence on the environment-induced dephasing in appropriate spin tunneling configurations. Our results unambiguously demonstrate that the information backaction of one conductor can substantially change the statistical fluctuations of the other even for noninvasive measurements, which may serve as a sensitive detection protocol in quantum metrology.

The rest of the paper is organized as follows. We start in Sec. II with an introduction of the ESR spin transport system monitored by a QPC detector, which is then followed in Sec. III by the description of the CCS in comparison with the unconditional FCS. Section IV is devoted to a detailed investigation of the unique CCS features of the ESR QPC system in appropriate parameter regimes. Finally, we conclude our findings in Sec. V.

II. MODEL SYSTEM

The system under investigation is schematically shown in Fig. 1(a), where a single QD is tunnel-coupled to a side electron reservoir. The QD is tuned in the Coulomb blockade regime such that double occupation is energetically prohibited and there is only one energy level involved in transport. The QD is subject to a magnetic field B_z in the z direction, which leads to the Zeeman splitting $\Delta = g_z\mu_{\rm B}B_z$, where g_z is the effective electron g factor in the z direction, and $\mu_{\rm B}$ is the Bohr magneton. Furthermore, an additional rotating magnetic field is applied in the x-y plane $B_\parallel(t) = B_\parallel\cos(\Omega t)\hat{e}_x + B_\parallel\sin(\Omega t)\hat{e}_y$, where the oscillation frequency Ω is tuned close to the Zeeman splitting Δ, leading to the well-known ESR and enabling spin flipping in the QD. The Fermi energy of the side electrode is tuned in the middle of the two Zeeman sublevels. At low temperatures, a spin-up electron can only tunnel into the QD from the side electrode, which is pumped to the higher energy level with a flipped spin orientation before it tunnels out to the side reservoir, leading thus to an ESR-pumped spin

current. The entire system Hamiltonian reads

$$H_{\rm T}(t) = H_{\rm S}(t) + H_{\rm B} + H_{\rm I}. \tag{1}$$

Here, $H_{\rm S}(t)$ denotes the Hamiltonian of the QD exposed to the magnetic field

$$H_{\rm S}(t) = \frac{\Delta}{2}(d_\downarrow^\dagger d_\downarrow - d_\uparrow^\dagger d_\uparrow) + U d_\uparrow^\dagger d_\uparrow d_\downarrow^\dagger d_\downarrow + \gamma_{\rm RF}(d_\uparrow^\dagger d_\downarrow e^{{\rm i}\Omega t} + d_\downarrow^\dagger d_\uparrow e^{-{\rm i}\Omega t}), \tag{2}$$

where d_σ ($d_\sigma^\dagger$) is the annihilation (creation) operator of an electron with spin $\sigma = \{\uparrow, \downarrow\}$ in the QD and $\gamma_{\rm RF} = g_\parallel \mu_{\rm B} B_\parallel$ is the ESR Rabi frequency, with $g_\parallel$ the electron g-factor in the parallel direction. Double occupation on the QD costs an intradot Coulomb charging energy U, which will be assumed to be infinitely large in the following ($U \to \infty$) such that double occupation on the QD is energetically prohibited.

The second term describes the side electron reservoir, modeled as a collection of noninteracting electrons

$$H_{\rm B} = \sum_k \sum_{\sigma=\uparrow,\downarrow} \varepsilon_{k\sigma} c_{k\sigma}^\dagger c_{k\sigma}, \tag{3}$$

where $c_{k\sigma}^\dagger (c_{k\sigma})$ is the creation (annihilation) operator of a spin-σ electron with momentum k in the side reservoir. The electron reservoir is in thermal equilibrium described by the Fermi distribution $f(\omega) = \{1 + e^{\beta(\omega-\mu_0)}\}^{-1}$, where $\beta = (k_{\rm B}T)^{-1}$ is the inverse temperature and μ_0 is the chemical potential in the middle of the spin-up and spin-down sublevels.

Electron tunneling between the QD and the side reservoir is described by

$$H_{\rm I} = \sum_{k,\sigma=\uparrow,\downarrow} (t_\sigma^* c_{k\sigma}^\dagger d_\sigma + t_\sigma c_{k\sigma} d_\sigma^\dagger), \tag{4}$$

where t_σ is the spin-dependent tunneling amplitude. The tunnel coupling strength between the QD and the side reservoir is described by the intrinsic linewidth $\Gamma_\sigma(\omega) = 2\pi |t_\sigma|^2 \mathcal{D}_\sigma(\omega)$ for spin up ($\sigma = \uparrow$) or spin down ($\sigma = \downarrow$) electrons, where $\mathcal{D}_\sigma(\omega)$ is the spin-dependent density of the states. On one hand, the tunneling amplitude t_σ depends on the height and width of the tunneling barrier. On the other hand, the electrode may have a structured spin-dependent density of states. According to the Stoner model of ferromagnetism [36], there might be a strong asymmetry in the density of states $\mathcal{D}_\sigma(\omega)$ for up ($\sigma = \uparrow$) or down ($\sigma = \downarrow$) spins [37]. It provides the possibility for different asymmetries in spin dependent tunneling strength. For simplicity, in the following we assume the tunnel coupling strengths to be energy independent, i.e., $\Gamma_\sigma(\omega) = \Gamma_\sigma$.

A QPC is placed in the vicinity of the QD. Its conductance is sensitive to changes in the surrounding electrostatic environment, and thus can be utilized to sense the presence (or absence) of an extra electron in the QD. When the QD is empty (occupied), the QPC current is I_0 (I_1), with $I_1 < I_0$ due to Coulomb repulsion. At sufficient low temperatures ($k_{\rm B}T \ll \Delta$), only spin-up electrons can tunnel into the QD and spin-down electrons tunnel out. Typical simulations of the QPC currents are shown in Figs. 1(b) and 1(c) for $\Gamma_\uparrow \gg \Gamma_\downarrow$ and $\Gamma_\uparrow \ll \Gamma_\downarrow$, respectively, based on the quantum trajectory method [10,38–40]. A switching of the QPC current from I_0 to I_1 implies that a spin-up electron has tunneled into the QD. When the QPC current undergoes an opposite jump, a spin-down electron has tunneled out of the QD. It is this spin-to-charge conversion mechanism that enables the QPC measurement of spin-resolved tunneling events between the QD and the side reservoir. It should be noted that the QPC is unable to distinguish between different spin states in the QD, and thus does not give rise to measurement-induced dephasing. Nevertheless, we will show that even for such a noninvasive QPC detector, the measurement leads to a CCS which is substantially different from the unconditional FCS.

Experimentally, measurement of the CCS in the ESR-QPC system can be implemented by replacing the side electrode reservoir by two ferromagnetic terminals with the same chemical potential. If the two terminals feature fully but oppositely spin-polarized tunnelings, this setup can be equivalently mapped onto the model as shown in Fig. 1(a), with the advantage of adjusting the spin dependent tunnelings though each terminal in a controllable manner. It thus enables the measurement of the CCS for various ratios between the spin tunneling rates.

III. CONDITIONAL COUNTING STATISTICS

Before we discuss the CCS, it is instructive to describe the general idea of conventional FCS in mesoscopic transport. This helps to get a better understanding of the difference between the two.

A. Full counting statistics

The randomness in QD and QPC transport is characterized by the joint probability distribution $P_t(\boldsymbol{N})$ ($\boldsymbol{N} = \{N_\uparrow, N_\downarrow, N_{\rm q}\}$), which describes the joint probabilities of finding $N_\uparrow$ spin-$\uparrow$ electrons, $N_\downarrow$ spin-$\downarrow$ electrons through the QD, and $N_{\rm q}$ electrons through the QPC during the time interval $[0, t]$. The joint probability distribution can be obtained from

$$P_t(\boldsymbol{N}) = {\rm tr}[\rho^{(\boldsymbol{N})}(t)], \tag{5}$$

where tr$[\cdots]$ denotes the trace over the degrees of freedom of the reduced system, $\rho^{(\boldsymbol{N})}(t)$ is the $\boldsymbol{N}$-resolved reduced density matrix [41] satisfying $\rho(t) = \sum_{\boldsymbol{N}} \rho^{(\boldsymbol{N})}(t)$. Here, $\rho(t) = {\rm tr}_{\rm B}[\rho_{\rm T}(t)]$ is the unconditional reduced density matrix, with $\rho_{\rm T}(t)$ the density matrix of the entire system and ${\rm tr}_{\rm B}[\cdots]$ the trace over the reservoir's degree of freedom.

However, due to the time dependence of the system Hamiltonian in Eq. (2), it is difficult to deal with the dynamics of the reduced density matrix directly. One may either use Floquet theory [42–45] or work in a time rotating frame. Here we adopt the latter and introduce the total density matrix in the rotating frame

$$\varrho_{\rm T}(t) = e^{{\rm i}\frac{\Omega}{2}\boldsymbol{\sigma}_z t} \rho_{\rm T}(t) e^{-{\rm i}\frac{\Omega}{2}\boldsymbol{\sigma}_z t}, \tag{6}$$

where $\boldsymbol{\sigma}_z$ is a pseudospin operator defined as $\boldsymbol{\sigma}_z = d_\downarrow^\dagger d_\downarrow - d_\uparrow^\dagger d_\uparrow$. The equation of motion of $\varrho_{\rm T}(t)$ simply reads

$$\frac{d}{dt}\varrho_{\rm T}(t) = -{\rm i}[\mathcal{H}_{\rm T}(t), \varrho_{\rm T}], \tag{7}$$

where $\mathcal{H}_{\rm T}(t) = \mathcal{H}_{\rm S} + \mathcal{H}_{\rm B} + \mathcal{H}_{\rm I}(t)$ is the entire Hamiltonian in the time rotating frame. Each term, respectively, is given by

$$\mathcal{H}_{\rm S} = \frac{1}{2}\delta_{\rm ESR}\boldsymbol{\sigma}_z + \gamma_{\rm RF}\boldsymbol{\sigma}_x, \tag{8a}$$

$$\mathcal{H}_{\rm B} = H_{\rm B} = \sum_{k\sigma} \epsilon_{k\sigma} c^\dagger_{k\sigma} c_{k\sigma}, \tag{8b}$$

$$\mathcal{H}_{\rm I}(t) = \sum_k \left(e^{{\rm i}\frac{\Omega}{2}t} t^*_{k\uparrow} c^\dagger_{k\uparrow} d_\uparrow + e^{-{\rm i}\frac{\Omega}{2}t} t^*_{k\downarrow} c^\dagger_{k\downarrow} d_\downarrow\right) + {\rm H.c.}, \tag{8c}$$

where $\delta_{\rm ESR} = \Delta - \Omega$ is the ESR detuning and $\boldsymbol{\sigma}_x$ is a pseudospin operator defined as $\boldsymbol{\sigma}_x = d^\dagger_\uparrow d_\downarrow + d^\dagger_\downarrow d_\uparrow$. In the time rotating frame, the reduced system Hamiltonian becomes time independent, and the Hamiltonian for the electron reservoir remains the same. Yet, the tunneling between the QD and reservoir becomes time dependent, which will be eventually irrelevant under the usual second-order perturbation expansion.

In the rotating frame, the reduced density matrix $\varrho(t)$ can be obtained by tracing the entire system density matrix over the reservoir's degrees of freedom, i.e., $\varrho(t) = {\rm tr}_{\rm B}[\varrho_{\rm T}(t)]$. As shown below, we can further unravel it into $\varrho(t) = \sum_{\boldsymbol{N}} \varrho^{(\boldsymbol{N})}(t)$, where $\varrho^{(\boldsymbol{N})}(t)$ is the $\boldsymbol{N}$-resolved reduced density matrix in the rotating frame. The corresponding joint probability distribution in the rotating frame is thus given by

$$\begin{aligned} P'_t(\boldsymbol{N}) &= {\rm tr}[\varrho^{(\boldsymbol{N})}(t)] = {\rm tr}\left[e^{{\rm i}\frac{\Omega}{2}\boldsymbol{\sigma}_z t}\rho^{(\boldsymbol{N})}(t)e^{-{\rm i}\frac{\Omega}{2}\boldsymbol{\sigma}_z t}\right] = {\rm tr}[\rho^{(\boldsymbol{N})}(t)] \\ &= P_t(\boldsymbol{N}), \end{aligned} \tag{9}$$

which turns out to be exactly the same as the original probability function in Eq. (5). It is therefore justified to work in the time rotating frame. The joint cumulant generating function (CGF) $\mathcal{F}_t(\boldsymbol{\chi})$ can be obtained via [17,18,46,47]

$$e^{-\mathcal{F}_t(\boldsymbol{\chi})} = \sum_{\boldsymbol{N}} P_t(\boldsymbol{N}) e^{-{\rm i}\boldsymbol{N}\cdot\boldsymbol{\chi}} = {\rm tr}[\varrho(\boldsymbol{\chi}, t)], \tag{10}$$

where $\boldsymbol{\chi} = \{\chi_\uparrow, \chi_\downarrow, \chi_{\rm q}\}$ are the counting fields associated with the corresponding numbers of transferred particles $\boldsymbol{N} = \{N_\uparrow, N_\downarrow, N_{\rm q}\}$, and $\varrho(\boldsymbol{\chi}, t)$ is the $\boldsymbol{\chi}$-dressed reduced density matrix

$$\varrho(\boldsymbol{\chi}, t) = \sum_{\boldsymbol{N}} \varrho^{(\boldsymbol{N})}(t) e^{-{\rm i}\boldsymbol{N}\cdot\boldsymbol{\chi}}. \tag{11}$$

Under the usual second-order Born-Markov approximation, the $\boldsymbol{\chi}$-dressed reduced density matrix $\varrho(\boldsymbol{\chi}, t)$ satisfies the following quantum master equation:

$$\dot{\varrho}(\boldsymbol{\chi}, t) = \mathcal{L}(\boldsymbol{\chi})\varrho(\boldsymbol{\chi}, t). \tag{12a}$$

To be specific, in the Fock state representation of the QD: $|0\rangle$, $|\uparrow\rangle$, and $|\downarrow\rangle$, standing for no extra electrons, one extra spin-$\uparrow$ electron, and one extra spin-$\downarrow$ electron, respectively, the reduced density matrix can be reexpressed as a column vector $\varrho \equiv (\varrho_{00}, \varrho_{\uparrow\uparrow}, \varrho_{\downarrow\downarrow}, \varrho_{\uparrow\downarrow}, \varrho_{\downarrow\uparrow})$, where $\varrho_{aa} = \langle a|\rho|a\rangle$ denotes the probability of the QD in the state $|a\rangle$ $(a = 0, \uparrow, \downarrow)$ and $\varrho_{\uparrow\downarrow} = \langle\uparrow|\rho|\downarrow\rangle$ denotes the coherences in the spin basis. The other off-diagonal elements are dynamically decoupled and thus excluded. Then $\mathcal{L}(\boldsymbol{\chi})$ is explicitly given by

$$\mathcal{L}(\boldsymbol{\chi}) = \begin{pmatrix} I_0 h(\chi_{\rm q}) - \Gamma_\uparrow & 0 & \Gamma_\downarrow e^{{\rm i}\chi_\downarrow} & 0 & 0 \\ \Gamma_\uparrow e^{-{\rm i}\chi_\uparrow} & I_1 h(\chi_{\rm q}) & 0 & {\rm i}\gamma_{\rm RF} & -{\rm i}\gamma_{\rm RF} \\ 0 & 0 & I_1 h(\chi_{\rm q}) - \Gamma_\downarrow & -{\rm i}\gamma_{\rm RF} & {\rm i}\gamma_{\rm RF} \\ 0 & {\rm i}\gamma_{\rm RF} & -{\rm i}\gamma_{\rm RF} & I_1 h(\chi_{\rm q}) + {\rm i}\delta_{\rm ESR} - \Gamma_\varphi & 0 \\ 0 & -{\rm i}\gamma_{\rm RF} & {\rm i}\gamma_{\rm RF} & 0 & I_1 h(\chi_{\rm q}) - {\rm i}\delta_{\rm ESR} - \Gamma_\varphi \end{pmatrix}, \tag{12b}$$

where $h(\chi_{\rm q}) = e^{{\rm i}\chi_{\rm q}} - 1$. The diagonal terms $I_j h(\chi_{\rm q})$ describe counting of tunneling events through the QPC detector with the tunneling currents I_j depending on whether the QD is empty $(j = 0)$ or occupied $(j = 1)$. It can be derived from a microscopic theory in the large bias voltage regime with unidirectional transport [29].

One may also describe the coupling between the spin and an additional noisy environment, which, in a phenomenological method, leads to spin relaxation (with typical time T_1 in which an excited spin state relaxes to the thermal equilibrium) and spin dephasing (with T_2 the time for losing the phase coherence). In what follows, we assume $T_1 \to \infty$ in recognition of recent transport experiments [35,48] but allow for an environment-induced spin dephasing [49–51]. This enables us to investigate the influence of a finite environment-induced dephasing on the CCS. Yet, it should be stressed that the QPC measurement can only distinguish whether the QD is occupied or not [see the jumps in the QPC current in Figs. 1(b) and 1(c)]. It can not distinguish the two spin states $|\uparrow\rangle$ and $|\downarrow\rangle$, and thus does not cause any measurement-induced dephasing. Therefore $\Gamma_\varphi = \frac{1}{T_2} + \frac{\Gamma_\downarrow}{2}$ is the total dephasing rate with $\frac{1}{T_2}$ purely due to coupling to the environment, and $\frac{\Gamma_\downarrow}{2}$ arising from tunnel coupling between the QD and the side reservoir.

In the stationary limit, the CGF $\mathcal{F}_t(\boldsymbol{\chi})$ is given by [18,47,52] $\mathcal{F}_t(\boldsymbol{\chi}) = \lambda(\boldsymbol{\chi})t$, where $\lambda(\boldsymbol{\chi})$ is the unique eigenvalue of $\mathcal{L}(\chi)$ that satisfies $\lambda(\boldsymbol{\chi})|_{\boldsymbol{\chi}\to\boldsymbol{0}} \to 0$. All the cumulants can be obtained by taking derivatives of the $\lambda(\boldsymbol{\chi})$ with respect to the counting fields. For instance, simple expressions for the first cumulants of the QD and the QPC can be obtained, respectively, as

$$\begin{aligned} \langle\langle J_\downarrow\rangle\rangle &= \partial_{{\rm i}\chi_\downarrow}\lambda(\boldsymbol{\chi})|_{\boldsymbol{\chi}\to\boldsymbol{0}} = \frac{4\Gamma_\downarrow\Gamma_\uparrow\gamma^2_{\rm RF}\left(\Gamma_\downarrow + \frac{2}{T_2}\right)}{\mathcal{N}} \\ &= -\langle\langle J_\uparrow\rangle\rangle, \end{aligned} \tag{13a}$$

$$\langle\langle I_q\rangle\rangle = \partial_{{\rm i}\chi_{\rm q}}\lambda(\boldsymbol{\chi})|_{\boldsymbol{\chi}\to\boldsymbol{0}} = I_0\varrho^{\rm st}_{00} + I_1\varrho^{\rm st}_{11}, \tag{13b}$$

where I_0 (I_1) is the QPC current when the QD is in the absence (presence) of an extra electron, and $\varrho^{\rm st}_{00} = 4\Gamma_\downarrow\gamma^2_{\rm RF}(\Gamma_\downarrow + \frac{2}{T_2})/\mathcal{N}$ and $\varrho^{\rm st}_{11} = \varrho^{\rm st}_{\uparrow\uparrow} + \varrho^{\rm st}_{\downarrow\downarrow} = [\Gamma_\uparrow(\Gamma_\downarrow + \frac{2}{T_2})(\Gamma^2_\downarrow + 8\gamma^2_{\rm RF} + \Gamma_\downarrow\frac{2}{T_2}) + 4\Gamma_\downarrow\delta^2_{\rm ESR}]/\mathcal{N}$ are the stationary probabilities of finding an empty and occupied QD, respectively, with $\mathcal{N} = (\Gamma_\downarrow + \frac{2}{T_2})(4\gamma^2_{\rm RF}(\Gamma_\downarrow + 2\Gamma_\uparrow) + \Gamma_\downarrow\Gamma_\uparrow(\Gamma_\downarrow + \frac{2}{T_2})) + 4\Gamma_\downarrow\Gamma_\uparrow\delta^2_{\rm ESR}$

denoting the normalization constant which ensures the probability conservation $\varrho_{00}^{\rm st}+\varrho_{11}^{\rm st}=1$.

Analogously, one may obtain the second cumulants of the QD and the QPC as (for $\delta_{\rm ESR}=0$ and $T_2^{-1}\to\infty$)

$$\begin{aligned}\langle\langle I_\sigma^2\rangle\rangle &= \partial_{{\rm i}\chi_\downarrow}^2\lambda(\boldsymbol{\chi})|_{\boldsymbol{\chi}\to\mathbf{0}}\\ &= \langle\langle J_\downarrow\rangle\rangle\frac{16\gamma_{\rm RF}^4(\Gamma_\downarrow^2+4\Gamma_\uparrow^2)+\Gamma_\downarrow^2\Gamma_\uparrow^2\left(\Gamma_\downarrow^2-8\gamma_{\rm RF}^2\right)}{\mathcal{N}^2}\\ &= -\langle\langle J_\uparrow J_\downarrow\rangle\rangle, \qquad (14a)\\ \langle\langle I_q^2\rangle\rangle &= \partial_{{\rm i}\chi_{\rm q}}^2\lambda(\boldsymbol{\chi})|_{\boldsymbol{\chi}\to\mathbf{0}} = 2(I_0-I_1)^2\langle\langle J_\downarrow\rangle\rangle\\ &\quad\times\frac{64\gamma_{\rm RF}^4+4\Gamma_\downarrow^2\gamma_{\rm RF}^2+\Gamma_\downarrow^4}{\mathcal{N}^2}+2\langle\langle I_q\rangle\rangle, \qquad (14b)\end{aligned}$$

respectively. In the limit of a vanishing Rabi frequency ($\gamma_{\rm RF}\to 0$), spin pumping is strongly suppressed and the spin transport is thus blocked ($\langle\langle J_\sigma\rangle\rangle\to 0$). As a consequence, the noise of the spin current goes to zero ($\langle\langle J_\sigma^2\rangle\rangle\to 0$) and that of the QPC current reduces to its background noise, i.e., $\langle\langle I_q^2\rangle\rangle\to 2\langle\langle I_q\rangle\rangle$.

It should be stressed that the QPC is a noninvasive detector, i.e., its current depends on the QD occupation, while the QD dynamics is not influenced by the QPC current. This is explicitly shown in the current cumulants of the QD, which are independent of the QPC parameters, see, for instance, the lowest two cumulants in Eqs. (13a) and (14a). That means, on the level of ensemble average, the QPC measurements do not physically affect the state of the QD system. This becomes apparent if one sets $\chi_{\rm q}=0$ in Eq. (12b) the dynamics of the QD is completely independent of the QPC. Nevertheless, a particular detection outcome of the QPC gives rise to a conditional backaction on the QD state, due to the information which we acquire by the measurement. This statistical or information backaction [20–24] can reveal a number of novel effects. Indeed, the information backaction is not just a concept, but can be measured experimentally [25]. In the following, we will investigate essentially this information backaction of ESR-QPC system via conditional counting statistics.

B. Conditional counting statistics

We introduce the conditional probability distribution function $P_t(N_\uparrow,N_\downarrow|N_{\rm q})$ describing the probability of finding $N_\uparrow$ spin-↑ electrons and $N_\downarrow$ spin-↓ electrons have tunneled through the QD, given that $N_{\rm q}$ electrons have tunneled through the QPC during the time interval $[0,t]$. The conditional probability distributions (or equivalently their corresponding conditional counting statistics) play an essential role in the statistical analysis of the dynamics. The corresponding conditional CGF $\mathcal{F}_t(\chi_\uparrow,\chi_\downarrow|N_{\rm q})$ is given by

$$e^{\mathcal{F}_t(\chi_\uparrow,\chi_\downarrow|N_{\rm q})}=\sum_{N_\uparrow,N_\downarrow}P_t(N_\uparrow,N_\downarrow|N_{\rm q})e^{{\rm i}N_\uparrow\chi_\uparrow+{\rm i}N_\downarrow\chi_\downarrow}. \qquad (15)$$

The conditional moments can be obtained by taking the partial derivatives

$$\langle N_\uparrow^{k_\uparrow}(t)N_\downarrow^{k_\downarrow}(t)\rangle_{N_{\rm q}}=\partial_{{\rm i}\chi_\uparrow}^{k_\uparrow}\partial_{{\rm i}\chi_\downarrow}^{k_\downarrow}e^{\mathcal{F}_t(\chi_\uparrow,\chi_\downarrow|N_{\rm q})}|_{\chi_\uparrow,\chi_\downarrow\to 0}. \qquad (16)$$

Now the central task is to evaluate the conditional CGF $\mathcal{F}_t(\chi_\uparrow,\chi_\downarrow|N_{\rm q})$. According to Bayes's theorem, the conditional probability distribution function $P_t(N_\uparrow,N_\downarrow|N_{\rm q})$ can be expressed as

$$P_t(N_\uparrow,N_\downarrow|N_{\rm q})=\frac{P_t(\boldsymbol{N})}{P_t(N_{\rm q})}, \qquad (17)$$

where $P_t(N_{\rm q})$ is the marginal probability distribution of the electrons which have tunneled through the QPC. The joint probability distribution is given by $P_t(\boldsymbol{N})={\rm tr}[\varrho^{(\boldsymbol{N})}(t)]$ as shown in Eq. (9). Thereby, the particle-number-resolved reduced density matrix $\varrho^{(\boldsymbol{N})}(t)$ can be obtained via an inverse Fourier transform

$$\varrho^{(\boldsymbol{N})}(t)=\int_0^{2\pi}\frac{d\boldsymbol{\chi}}{(2\pi)^3}e^{-{\rm i}\boldsymbol{N}\cdot\boldsymbol{\chi}}\varrho(\boldsymbol{\chi},t), \qquad (18)$$

where the $\boldsymbol{\chi}$-dependent reduced density matrix satisfies the QME in Eq. (12a). By combining Eqs. (15)–(18), we find the spin-resolved conditional moments

$$\langle N_\uparrow^{k_\uparrow}N_\downarrow^{k_\downarrow}\rangle_{N_{\rm q}}=\partial_{{\rm i}\chi_\uparrow}^{k_\uparrow}\partial_{{\rm i}\chi_\downarrow}^{k_\downarrow}\int_0^{2\pi}\frac{d\chi_{\rm q}e^{-{\rm i}N_{\rm q}\chi_{\rm q}}}{2\pi P_t(N_{\rm q})}{\rm tr}[\varrho(\boldsymbol{\chi},t)]_{\chi_\uparrow,\chi_\downarrow\to 0}, \qquad (19)$$

where $\varrho(\boldsymbol{\chi},t)$ is the solution of the generalized quantum master equation (12).

Since an analytical solution of $\varrho(\boldsymbol{\chi},t)$ is not available, one might solve Eq. (12) numerically for all the counting fields and then perform the Fourier transform according to Eq. (19). Yet, we will not calculate the conditional moments in this way for two reasons. First, it is not necessary to evaluate the full dependence of the density matrix on the counting fields. What we need is the partial derivative of $\varrho(\boldsymbol{\chi},t)$ evaluated at the point $\chi_\uparrow=\chi_\downarrow=0$. Second, taking high order partial derivatives by using the numerical calculated $\varrho(\boldsymbol{\chi},t)$ may suffer from numerical instabilities. Therefore we introduce a spin-resolved auxiliary reduced density matrix

$$\varrho_{[k_\uparrow,k_\downarrow]}(\chi_{\rm q},t)\equiv\partial_{{\rm i}\chi_\uparrow}^{k_\uparrow}\partial_{{\rm i}\chi_\downarrow}^{k_\downarrow}\varrho(\boldsymbol{\chi},t)|_{\chi_\uparrow,\chi_\downarrow\to 0}\quad(k_\uparrow,k_\downarrow\geqslant 0), \qquad (20)$$

which is a generalization of the auxiliary density matrix approach in Refs. [27,53,54] that includes the spin degrees of freedom. Taking partial derivatives of Eq. (12a) with respect to the counting field $\chi_\uparrow$ by $k_\uparrow$ times and $\chi_\downarrow$ by $k_\downarrow$ times, we obtain the following coupled differential equations

$$\begin{aligned}\dot\varrho_{[0,0]} &= \mathcal{L}_{[0,0]}\varrho_{[0,0]}, \qquad (21a)\\ \dot\varrho_{[0,1]} &= \mathcal{L}_{[0,1]}\varrho_{[0,0]}+\mathcal{L}_{[0,0]}\varrho_{[0,1]}, \qquad (21b)\\ \dot\varrho_{[1,0]} &= \mathcal{L}_{[1,0]}\varrho_{[0,0]}+\mathcal{L}_{[0,0]}\varrho_{[1,0]}, \qquad (21c)\\ \dot\varrho_{[0,2]} &= \mathcal{L}_{[0,2]}\varrho_{[0,0]}+2\mathcal{L}_{[0,1]}\varrho_{[0,1]}+\mathcal{L}_{[0,0]}\varrho_{[0,2]}, \qquad (21d)\\ \dot\varrho_{[1,1]} &= \mathcal{L}_{[1,1]}\varrho_{[0,0]}+\mathcal{L}_{[1,0]}\varrho_{[0,1]}+\mathcal{L}_{[0,1]}\varrho_{[1,0]}\\ &\quad+\mathcal{L}_{[0,0]}\varrho_{[1,1]}, \qquad (21e)\\ \dot\varrho_{[2,0]} &= \mathcal{L}_{[2,0]}\varrho_{[0,0]}+2\mathcal{L}_{[1,0]}\varrho_{[1,0]}+\mathcal{L}_{[0,0]}\varrho_{[2,0]}, \qquad (21f)\\ \cdots &= \cdots \qquad (21g)\\ \dot\varrho_{[k_\uparrow,k_\downarrow]} &= \mathcal{L}_{[k_\uparrow,k_\downarrow]}\varrho_{[0,0]}+k_\downarrow\mathcal{L}_{[k_\uparrow-1,k_\downarrow]}\varrho_{[1,0]}\\ &\quad+k_\uparrow\mathcal{L}_{[k_\uparrow,k_\downarrow-1]}\varrho_{[0,1]}+k_\uparrow k_\downarrow\mathcal{L}_{[k_\uparrow-1,k_\downarrow-1]}\varrho_{[1,1]}\\ &\quad+\cdots+\mathcal{L}_{[0,0]}\varrho_{[k_\uparrow,k_\downarrow]}, \qquad (21h)\end{aligned}$$

where, for simplicity, we have introduced the notation

$$\mathcal{L}_{[k_\uparrow,k_\downarrow]}(\chi_{\rm q})\equiv\partial_{{\rm i}\chi_\uparrow}^{k_\uparrow}\partial_{{\rm i}\chi_\downarrow}^{k_\downarrow}\mathcal{L}(\boldsymbol{\chi})|_{\chi_\uparrow,\chi_\downarrow\to 0}\quad(k_\uparrow,k_\downarrow\geqslant 0). \qquad (22)$$

By representing the density matrix as a column vector $\boldsymbol{\mu}(\chi_{\rm q},t)\equiv(\varrho_{[0,0]},\varrho_{[0,1]},\varrho_{[1,0]},\cdots,\varrho_{[k_\uparrow,k_\downarrow]})^{\rm T}$, Eq. (21) can be reexpressed as

$$\dot{\boldsymbol{\mu}}(\chi_{\rm q},t)=\mathcal{Z}(\chi_{\rm q})\boldsymbol{\mu}(\chi_{\rm q},t), \tag{23}$$

where the super operator $\mathcal{Z}(\chi_{\rm q})$ is given by

$$\mathcal{Z}(\chi_{\rm q})=\begin{pmatrix}
\mathcal{L}_{[0,0]} & 0 & 0 & 0 & 0 & 0 & \cdots & 0\\
\mathcal{L}_{[0,1]} & \mathcal{L}_{[0,0]} & 0 & 0 & 0 & 0 & \cdots & 0\\
\mathcal{L}_{[1,0]} & 0 & \mathcal{L}_{[0,0]} & 0 & 0 & 0 & \cdots & 0\\
\mathcal{L}_{[0,2]} & 2\mathcal{L}_{[0,1]} & 0 & \mathcal{L}_{[0,0]} & 0 & 0 & \cdots & 0\\
\mathcal{L}_{[1,1]} & \mathcal{L}_{[1,0]} & \mathcal{L}_{[0,1]} & 0 & \mathcal{L}_{[0,0]} & 0 & \cdots & 0\\
\mathcal{L}_{[2,0]} & 0 & 2\mathcal{L}_{[1,0]} & 0 & 0 & \mathcal{L}_{[0,0]} & \cdots & 0\\
\vdots & \vdots & \vdots & \vdots & \vdots & \vdots & \ddots & \vdots\\
\mathcal{L}_{[k_\uparrow,k_\downarrow]} & k_\uparrow\mathcal{L}_{[k_\uparrow,k_\downarrow-1]} & k_\downarrow\mathcal{L}_{[k_\uparrow-1,k_\downarrow]} & (k_\downarrow-1)\mathcal{L}_{[k_\uparrow-2,k_\downarrow]} & k_\downarrow k_\uparrow\mathcal{L}_{[k_\uparrow-1,k_\downarrow-1]} & (k_\uparrow-1)\mathcal{L}_{[k_\uparrow,k_\downarrow-2]} & \cdots & \mathcal{L}_{[0,0]}
\end{pmatrix}. \tag{24}$$

We assume that the counting starts at $t=0$, where the system has reached its stationary state such that $\varrho^{(N)}(t=0)=\varrho_{\rm st}\delta_{N_\uparrow,0}\delta_{N_\downarrow,0}\delta_{N_{\rm q},0}$ and thus $\varrho_{[0,0]}(\chi_{\rm q},t=0)=\varrho(\boldsymbol{\chi},t=0)|_{\chi_\uparrow,\chi_\downarrow\to0}=\varrho_{\rm st}$, with $\varrho_{\rm st}$ denoting the stationary reduced density matrix. All the higher tier auxiliary density matrices vanish at $t=0$, i.e., $\varrho_{[k_\uparrow,k_\downarrow]}(\chi_{\rm q},t=0)=\partial_{{\rm i}\chi_\uparrow}^{k_\uparrow}\partial_{{\rm i}\chi_\downarrow}^{k_\downarrow}\varrho(\boldsymbol{\chi},t=0)|_{\chi_\uparrow,\chi_\downarrow\to0}=0$ for $k_\uparrow+k_\downarrow\geqslant1$, meaning Eq. (23) is solved with the initial condition $\boldsymbol{\mu}(\chi_{\rm q},t=0)\equiv(\varrho_{\rm st},0,\ldots,0)^{\rm T}$. Inspection of Eq. (24) reveals that an arbitrary tier auxiliary density matrix is only coupled to lower tier density matrices, such that they form a closed set of equations. Thus, one only has to solve Eq. (23) up to the tier corresponding to the desired conditional moment.

By substituting the solution $\varrho_{[k_\uparrow,k_\downarrow]}(\chi_{\rm q},t)$ into Eq. (19), one eventually arrives at the corresponding spin-resolved conditional moments, from which one can equivalently obtain the conditional cumulants. For instance, the lowest two spin-resolved conditional cumulants are given by

$$\langle\langle N_\sigma\rangle\rangle_{N_{\rm q}}=\langle N_\sigma\rangle_{N_{\rm q}}, \tag{25a}$$

$$\left\langle\left\langle N_\sigma^2\right\rangle\right\rangle_{N_{\rm q}}=\left\langle N_\sigma^2\right\rangle_{N_{\rm q}}-\langle N_\sigma\rangle_{N_{\rm q}}^2. \tag{25b}$$

Higher-order conditional cumulants can be obtained in an analogous manner.

IV. RESULTS AND DISCUSSION

A. Conditional spin-resolved current cumulants

The spin-down conditional current ($\langle\langle N_\downarrow\rangle\rangle_{N_{\rm q}}/t_{\rm m}$) is plotted in Fig. 2 for various ESR detunings with a given measurement time $t_{\rm m}$. The spin-up counterpart satisfies $\langle\langle N_\uparrow\rangle\rangle_{N_{\rm q}}=-\langle\langle N_\downarrow\rangle\rangle_{N_{\rm q}}$ and is not displayed in Fig. 2. When the QD is dominantly occupied (empty), the QPC current approaches $I_1=80\Gamma$ ($I_0=120\Gamma$). To appropriately include the width of the probability distribution of the QPC current which is approximately 5Γ, we therefore plot the spin-resolved conditional counting statistics of the QD within the regime $75\Gamma\leqslant N_{\rm q}/t_{\rm m}\leqslant125\Gamma$. For comparison, we have also depicted the unconditional currents by horizontal lines in Fig. 2(a), where each color corresponds to the same parameters as the conditional currents. These unconditional currents obtained by averaging the conditioned expectation values over $N_{\rm q}$ are in striking agreement with the theoretical predictions.

Let us first consider the situation $\Gamma_\uparrow\gg\Gamma_\downarrow$ ($\Gamma_\uparrow=0.9\Gamma$ and $\Gamma_\downarrow=0.1\Gamma$, where $\Gamma=\Gamma_\uparrow+\Gamma_\downarrow$ is set as the unit of energy throughout this work). In order to obtain a meaningful statistics of spin-resolved currents, we employ a large measurement time $t_{\rm m}=20\Gamma^{-1}$. For the above defined parameters, the QD is most of the time occupied such that the QPC current distribution is peaked roughly at $N_{\rm q}/t_{\rm m}\approx80\Gamma$ within the regime $75\Gamma<N_{\rm q}/t_{\rm m}<100\Gamma$. For $100\Gamma<N_{\rm q}/t_{\rm m}<125\Gamma$, the QPC current probability $P_{t_{\rm m}}(N_{\rm q})$ and the joint probability $P_{t_{\rm m}}(N_\downarrow,N_{\rm q})$ are both quite small (but roughly on the same order). According to Bayes's theorem in Eq. (17), we thus observe a finite value in the spin-resolved conditional current through the QD. Although at small measurement times the QPC currents have relatively broader distributions, the corresponding spin-resolved conditional currents are qualitatively the same (not shown here explicitly).

It is observed that in contrast to the unconditional current cumulants in Eqs. (13a) and (14a) which are independent of the QPC detection current, the conditional counterparts are apparently sensitive to the QPC current. In comparison with the conditional charge transport through a single QD [25], the spin-resolved conditional current exhibits unique correlations. First, we find a finite spin current even at $N_{\rm q}/t_{\rm m}=I_0$ and $N_{\rm q}/t_{\rm m}=I_1$, the QPC endpoint currents corresponding to an empty and occupied QD, respectively. The nonvanishing conditional current is attributed to the QPC detector shot noise. If one formally neglects the QPC shot noise (by expanding $e^{{\rm i}\chi_{\rm q}}$ up to the first order in $\chi_{\rm q}$), the conditional spin current would vanish at the endpoints. An increase of the ESR detuning suppresses the QPC shot noise (see the inset in Fig. 2), which leads thus to a reduction of the spin-down conditional current, particularly prominent at the endpoint $N_{\rm q}/t_{\rm m}=I_1$. The second unique feature is that, different from the semicircular conditional charge current in a single QD [25], the spin-resolved conditional cumulant $\langle\langle N_\downarrow\rangle\rangle_{N_{\rm q}}$ is unambiguously asymmetric. Especially, a radical change is observed for a large ESR

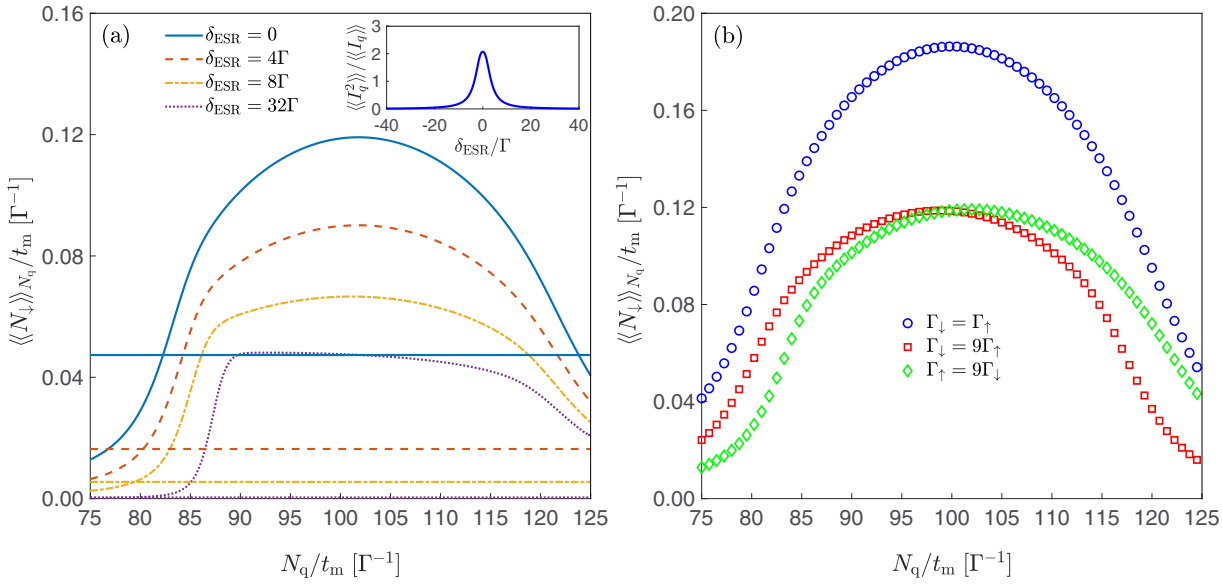

FIG. 2. (a) The spin-resolved conditional current vs the QPC detector current for various ESR detunings with very asymmetric spin tunneling rates $\Gamma_\uparrow = 9\Gamma_\downarrow$. For comparison, the corresponding unconditional spin-resolved currents $\langle\langle J_\downarrow\rangle\rangle$ are also plotted by the curves with the same color. (b)The spin-resolved conditional current vs the QPC detector current for $\delta_{\rm ESR}=0$ with $\Gamma_\uparrow=\Gamma_\downarrow$ (circles), $\Gamma_\downarrow=9\Gamma_\uparrow$ (squares), and $\Gamma_\uparrow=9\Gamma_\downarrow$ (diamonds). The other plotting parameters are $\gamma_{\rm RF}=2\Gamma$, $T_2^{-1}=0$, $I_0=120\Gamma$, $I_1=80\Gamma$, and a measurement time $t_m=20\Gamma^{-1}$, where $\Gamma=\Gamma_\uparrow+\Gamma_\downarrow$ is set as unit of energy. (Inset) Unconditional QPC shot noise vs ESR detuning.

detuning: The semicircle-like behavior turns into a steplike behavior such that the maximum is apparently shifted towards a lower QPC current, see the dotted curve for $\delta_{\rm ESR}=32\Gamma$ in Fig. 2.

To elucidate this unique asymmetric correlation, we expand the system Hamiltonian in Eq. (8a) as

$$\tilde{\mathcal{H}}_{\rm S}=\tfrac{1}{2}\tilde{E}(|+\rangle\langle+|-|-\rangle\langle-|), \tag{26}$$

where $\tilde{E}=(\delta_{\rm ESR}^2+4\gamma_{\rm RF}^2)^{\frac{1}{2}}$ is the eigenenergy splitting, and $|+\rangle$ and $|-\rangle$ are the eigenstates given by

$$|+\rangle=\sin\left(\frac{\theta}{2}\right)|\uparrow\rangle+\cos\left(\frac{\theta}{2}\right)|\downarrow\rangle, \tag{27a}$$

$$|-\rangle=\cos\left(\frac{\theta}{2}\right)|\uparrow\rangle-\sin\left(\frac{\theta}{2}\right)|\downarrow\rangle. \tag{27b}$$

Here θ is introduced via $\sin\theta=2\gamma_{\rm RF}/\tilde{E}$. As a result, the tunnel-coupling Hamiltonian in Eq. (8c) becomes

$$\begin{aligned}\tilde{\mathcal{H}}_{\rm I}(t)=\sum_k\Bigg\{&\Bigg[e^{i\frac{\Omega}{2}t}t_{k\uparrow}^*\sin\left(\frac{\theta}{2}\right)c_{k\uparrow}^\dagger\\&+e^{-i\frac{\Omega}{2}t}t_{k\downarrow}^*\cos\left(\frac{\theta}{2}\right)c_{k\downarrow}^\dagger\Bigg]|0\rangle\langle+|\\&+\Bigg[e^{i\frac{\Omega}{2}t}t_{k\uparrow}^*\cos\left(\frac{\theta}{2}\right)c_{k\uparrow}^\dagger\\&-e^{-i\frac{\Omega}{2}t}t_{k\downarrow}^*\sin\left(\frac{\theta}{2}\right)c_{k\downarrow}^\dagger\Bigg]|0\rangle\langle-|\Bigg\}+\text{H.c.}\end{aligned} \tag{28}$$

It is now apparent that the ESR system can be mapped onto a two-level system tunnel-coupled to fully spin-up polarized and spin-down polarized electrodes, as schematically shown in Fig. 3. The tunneling amplitudes are effectively modulated by the ESR detuning and Rabi frequency via θ. Again, the time dependence in Eq. (28) is irrelevant under the second order expansion and thus suppressed in Fig. 3.

For a vanishing ESR detuning ($\delta_{\rm ESR}\to 0$, $\theta\to\frac{\pi}{2}$), electrons transfer from the spin-up polarized electrode to the two states "$|+\rangle$" and "$|-\rangle$" with comparable rates as shown in Fig. 3(a), where the thickness of the arrows indicates the magnitude of the corresponding tunneling rates. Likewise, the tunneling rates between the spin-down polarized electrode and the states "$|+\rangle$" and "$|-\rangle$" are comparable. Yet, for $\Gamma_\uparrow\gg\Gamma_\downarrow$ it means that tunneling rates between the spin-up polarized electrode and the system are much stronger than those between the spin-down polarized electrode and the system, implying that the system is most of the time occupied. To quantitatively explain the asymmetry in the spin-resolved conditional current, we depict in Fig. 4 the conditional probabilities $P(N_\downarrow|N_q)$ for given QPC currents $N_q/t_m=80\Gamma$ and $N_q/t_m=120\Gamma$ with different spin tunneling asymmetries $\Gamma_\uparrow=9\Gamma_\downarrow$ and $\Gamma_\downarrow=9\Gamma_\uparrow$, respectively. For $\Gamma_\uparrow=9\Gamma_\downarrow$, the conditional probability for $N_q/t_m=120\Gamma$ [Fig. 4(b)] shows a larger average value than that for $N_q/t_m=80\Gamma$ [Fig. 4(a)]. This is the reason that we observe a larger conditional current at $N_q/t_m=120\Gamma$ than that at $N_q/t_m=80\Gamma$, as shown by the diamonds in Fig. 2(b). Similar analysis applies to the opposite case $\Gamma_\downarrow=9\Gamma_\uparrow$ in Fig. 4(c) and Fig. 4(d), which explains a larger conditional current at $N_q/t_m=80\Gamma$ than that at $N_q/t_m=120\Gamma$ [cf. the squares in Fig. 2(b)].

In the limit of a large ESR detuning ($\delta_{\rm ESR}\gg\gamma_{\rm RF}$, $\theta\to 0$), the coupling between spin-up polarized electrode to the state "$|+\rangle$" as well as that between spin-down polarized electrode to the state "$|-\rangle$" have almost vanishing contributions, such that the system can be mapped onto a coupled two-level system, where the electrons tunnel via the following path: Spin-up polarized electrode $\rightleftharpoons|-\rangle\rightleftharpoons|+\rangle\rightleftharpoons$ spin-down polarized electrode, as indicated by the arrows in Fig. 3(d). In

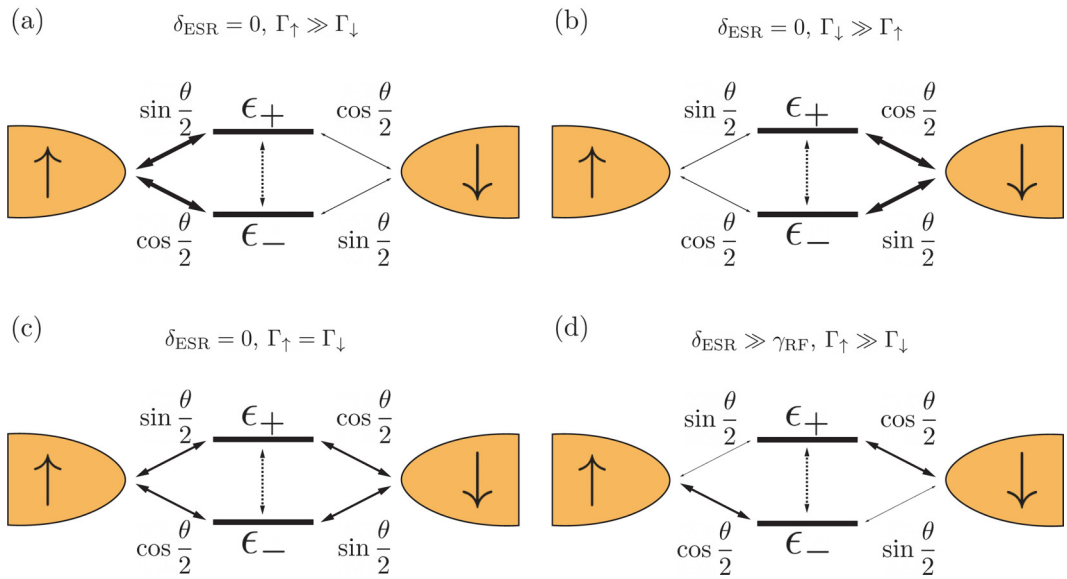

FIG. 3. (a) Different spin transport configurations in the eigenstate basis for (a) $\delta_{\rm ESR}=0$ and $\Gamma_\uparrow\gg\Gamma_\downarrow$, (b) $\delta_{\rm ESR}=0$ and $\Gamma_\downarrow\gg\Gamma_\uparrow$, (c) $\delta_{\rm ESR}=0$ and $\Gamma_\downarrow=\Gamma_\uparrow$, and (d) $\delta_{\rm ESR}\gg\gamma_{\rm RF}$ and $\Gamma_\uparrow\gg\Gamma_\downarrow$. The ESR detuning, together with the tunneling rates Γ_σ can modulate the tunneling strength in the eigenbasis, which is indicated by the thickness of the arrows in each panel.

the limit of strong spin tunneling asymmetry ($\Gamma_\uparrow\gg\Gamma_\downarrow$), the electron has a very low probability to tunnel out, such that it will stay in the eigenstate $|+\rangle$ for a long time. This shows the advantage of the eigenbasis picture (Fig. 3) in that it reveals not only the occupation of the quantum dot, but also specifically which eigenstate is dominantly occupied, as well as a more detailed understanding of the spin transport processes. In this case, a large $\delta_{\rm ESR}$ leads to a prominent suppression of the QPC shot noise (cf. the inset in Fig. 2), which gives rise to a strong inhibition of the spin-resolved conditional current through the QD.

The occurrence of the step-like behavior in Fig. 2 can be explained as follows. During the measurement time $t_{\rm m}=20\Gamma^{-1}$, at most one electron can tunnel out of the quantum dot. The probability for multiple tunnel events is strongly suppressed because of the large detuning, i.e., $P(N_\uparrow>1\mid N_{\rm q})\approx 0$. Moreover, $P(N_\uparrow=0\mid N_{\rm q}\gg I_1t_{\rm m})\approx 0$ if $N_{\rm q}$ is significantly larger than $I_1t_{\rm m}$. For this reason, we conclude that $P(N_\uparrow=1\mid N_{\rm q}\gg I_1t_{\rm m})\approx 1$, thus leading to the plateau observed in Fig. 2(a). Accordingly, the noise is increasingly suppressed for $N_{\rm q}/t_{\rm m}>95\Gamma$ as can be seen in Figs. 5(a), 6(b), and 7(b) for increasing detunings, as the probability distribution converges

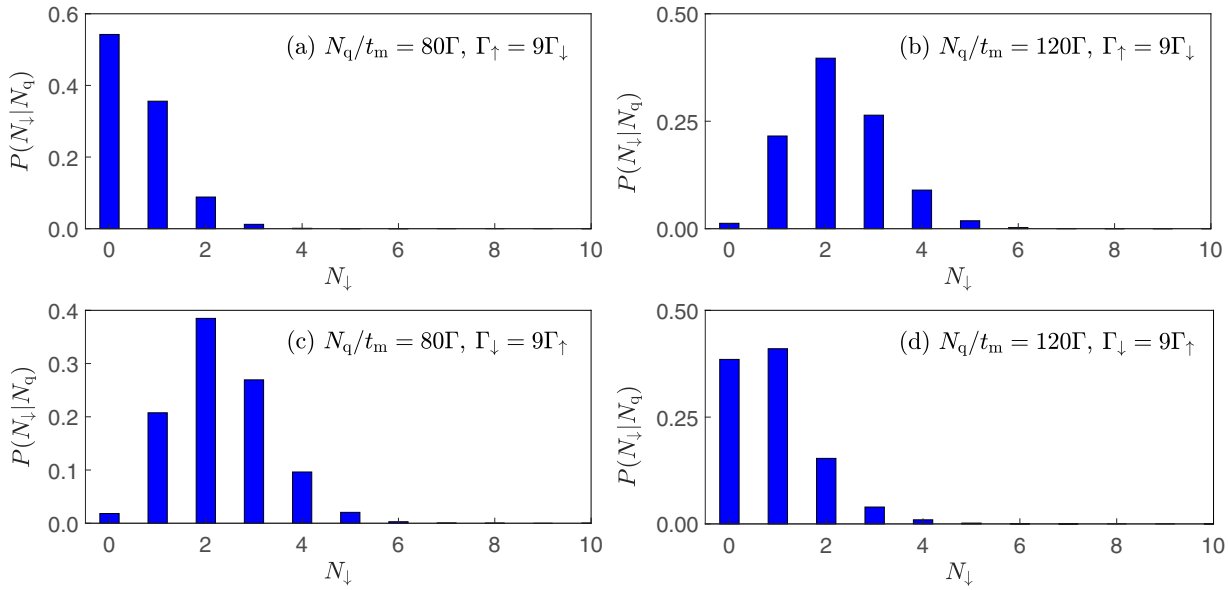

FIG. 4. The conditional probability distributions $P(N_\downarrow|N_{\rm q})$ for a given QPC current $N_{\rm q}/t_{\rm m}=80\Gamma$ with (a) $\Gamma_\uparrow=9\Gamma_\downarrow$ and (c) $\Gamma_\downarrow=9\Gamma_\uparrow$, as well as these for $N_{\rm q}/t_{\rm m}=120\Gamma$ with (b) $\Gamma_\uparrow=9\Gamma_\downarrow$ and (d) $\Gamma_\downarrow=9\Gamma_\uparrow$, respectively. The other plotting parameters are: $\gamma_{\rm RF}=2\Gamma$, $T_2^{-1}=0$, $\delta_{\rm ESR}=0$, and a measurement time $t_{\rm m}=20\Gamma^{-1}$.

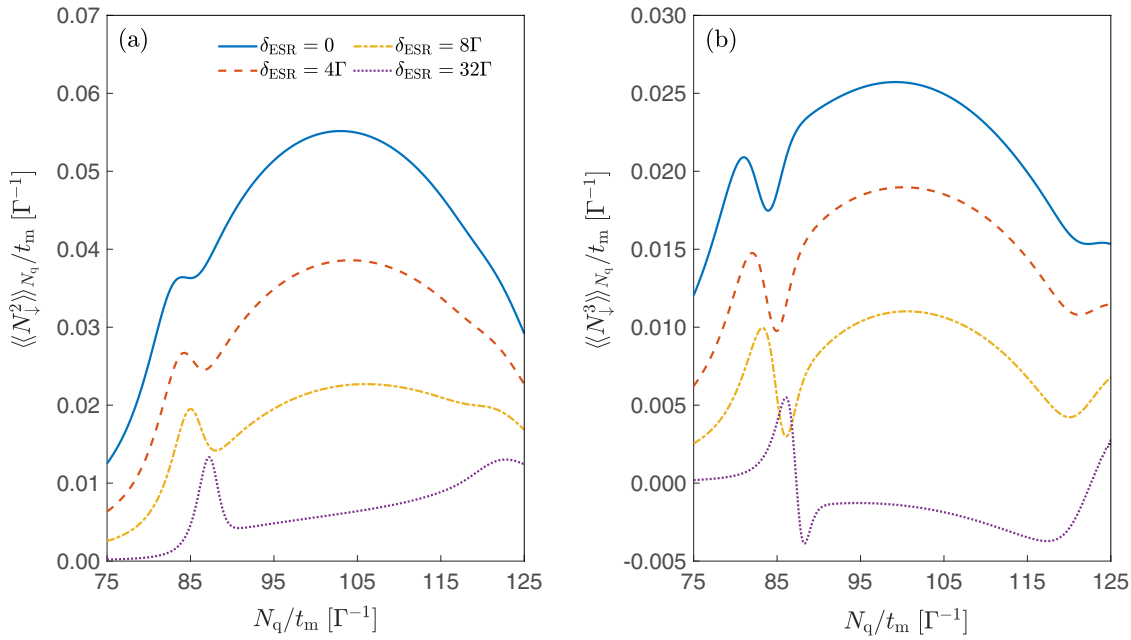

FIG. 5. (a) Spin-resolved conditional shot noise and (b) skewness vs QPC detection current for various ESR detunings in the absence of environment-induced dephasing ($\frac{1}{T_2}\to 0$). The other plotting parameters are the same as those in Fig. 2.

to $P(N_\uparrow \mid N_{\rm q}\gg I_1 t_{\rm m})\approx\delta_{N_\uparrow,1}$ in this regime. This leads to a formation of a peak in the noise around $N_{\rm q}/t_{\rm m}=90\Gamma$.

The intimate correlation between spin transport and QPC detection is much more sensitively reflected in the higher-order conditional cumulants, such as the conditional shot noise $\langle\langle N_\downarrow^2\rangle\rangle_{N_{\rm q}}$ and skewness $\langle\langle N_\downarrow^3\rangle\rangle_{N_{\rm q}}$, shown in Figs. 5(a) and 5(b), respectively. For instance, the conditional shot noise is much more asymmetric than the conditional current for the same parameters in the conditional current. An increase in ESR detuning leads to a general suppression of the conditional shot noise. The semicircular-like behavior gradually vanishes and prominent peaks appear at the position where the conditional current shows a step-like structure. For a sufficient large ESR detuning (cf. the dotted curve for $\delta_{\rm ESR}=32\Gamma$), the local maximum turns into a global one. The conditional skewness is more susceptible, which shows a prominent dip even at $\delta_{\rm ESR}=0$. As the ESR detuning grows, the dip gradually evolves into an inflexion. For sufficient large $\delta_{\rm ESR}$, the conditional skewness is remarkably suppressed and becomes even negative when the QPC current exceeds the critical value, as shown by the dotted curve in Fig. 5(b).

The influence of the Rabi frequency on the spin-resolved CCS is investigated in Fig. 6. For small Rabi frequencies,

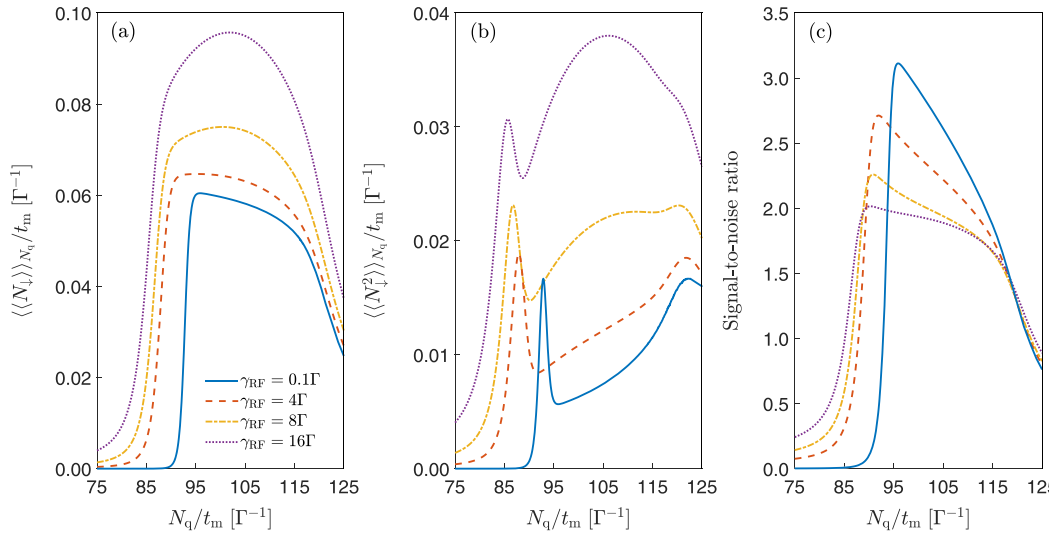

FIG. 6. (a) Spin-resolved conditional current, (b) noise, and (c) signal-to-noise ratio vs QPC detection current for various Rabi frequencies with $\delta_{\rm ESR}=32\Gamma$. The other plotting parameters are the same as those in Fig. 2.

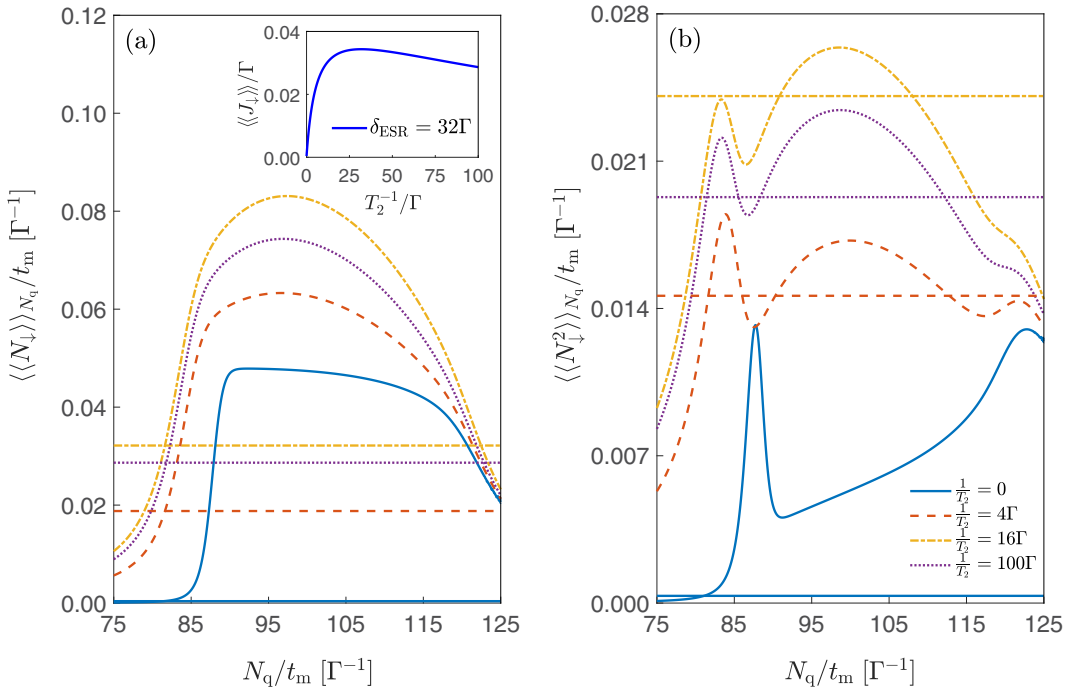

FIG. 7. (a) Spin-resolved conditional current and (b) shot noise vs QPC detection current for various environment-induced dephasing rates ($\frac{1}{T_2}$) with ESR detuning $\delta_{\rm ESR} = 32\Gamma$. The horizontal lines are the corresponding unconditional currents and noises. Inset: The unconditional spin-resolved current $J_\downarrow$ versus dephasing rate $\frac{1}{T_2}$ for $\delta_{\rm ESR} = 32\Gamma$. The other plotting parameters are the same as those in Fig. 2.

the conditional current $\langle\langle N_\downarrow\rangle\rangle_{N_{\rm q}}/t_{\rm m}$ shows prominent step-like structures and the conditional noise $\langle\langle N_\downarrow^2\rangle\rangle_{N_{\rm q}}/t_{\rm m}$ exhibits a pronounced peak due to the increasing detunings. The effect of an increasing $\gamma_{\rm RF}$ is twofold. First, as the Rabi frequency increases, the step of the conditional current and the peak of the noise both shift towards low $N_{\rm q}/t_{\rm m}$. In this case, the spin-down electron tends to dwell on the QD for a longer time before it tunnels out to the electrode, leading thus to a longer plateau. Second, both $\langle\langle N_\downarrow\rangle\rangle_{N_{\rm q}}/t_{\rm m}$ and $\langle\langle N_\downarrow^2\rangle\rangle_{N_{\rm q}}/t_{\rm m}$ increase with rising Rabi frequency in general. This is due to the fact that an increase in $\gamma_{\rm RF}$ leads to a growing θ, similar to a decrease in ESR detuning. Thus, as $\gamma_{\rm RF}$ increases, the steplike structure disappears, just as an decrease in $\delta_{\rm ESR}$ does. It is worthwhile to mention that the CCS and the signal-to-noise ratio $[\langle\langle N_\downarrow\rangle\rangle_{N_{\rm q}}/(\langle\langle N_\downarrow^2\rangle\rangle_{N_{\rm q}})^{1/2}]$ both exhibit high sensitivity to the Rabi frequency, showing their potential to probe the magnetic field in the x-y plane, which may serve as a promising protocol for quantum metrology.

So far, we have analyzed the CCS in the absence of dephasing, which is justified by the fact that the QPC detector does not distinguish the two spin states. In order to quantitatively elucidate the effect of finite dephasing on the CCS, we allow for finite environment-induced dephasing in Eq. (12). The spin resolved conditional cumulants for various dephasing rates ($\frac{1}{T_2}$) with a large ESR detuning ($\delta_{\rm ESR} = 32\Gamma$) are plotted in Fig. 7. For $\frac{1}{T_2} \to 0$, the conditional spin current shows a step-like structure and the conditional spin current noise exhibits a prominent peak as shown by the solid curves in Fig. 7, see also Figs. 2 and 5(a). A small increase in $\frac{1}{T_2}$ gives rise to a general enhancement of the conditional current and noise, cf. the dashed and dash-dotted curves in Figs. 7(a) and 7(b), respectively. In the regime of large depahsing rates, both conditional current and noise decreases with $\frac{1}{T_2}$, see the dotted curve in Figs. 7(a) and 7(b) for $\frac{1}{T_2} = 100\Gamma$. The conditional and uncondtional current and noise show qualitatively similar behavior with the dephasing rate, see, for instance, the unconditional current in the inset of Fig. 7(a). Here, both conditional current and unconditional current [see Eq. (13a)] are sensitive to the dephasing. This shows a striking difference in comparison with the unconditional current through a DQD system, which is independent of dephasing [55,56]. The unconditional currents and noises obtained from averaging the conditioned expectation values are also plotted by the horizontal lines for comparison. It is found that they are in striking agreement with the results using the unconditional master equation (not shown explicitly).

B. Conditional QPC current cumulants

Let us now turn the perspective around and consider the QD as a detector and investigate the conditional QPC current fluctuations, given an observation of the QD spin-resolved current. In the low-temperature regime, they can be theoretically evaluated following a similar procedure as described in Sec. IV. In each trajectory, a jump down (up) of the QPC current indicates that an electron has tunneled into (out of) the QD. Using this deterministic correlation, we obtain the number of tunneled electrons through the QD by counting the number of jumps during a given measurement time $t_{\rm m}$. By utilizing a large number of single trajectories with the same measurement time $t_{\rm m}$, one is able to obtain the statistics of the QPC current for a given number of electrons transferred

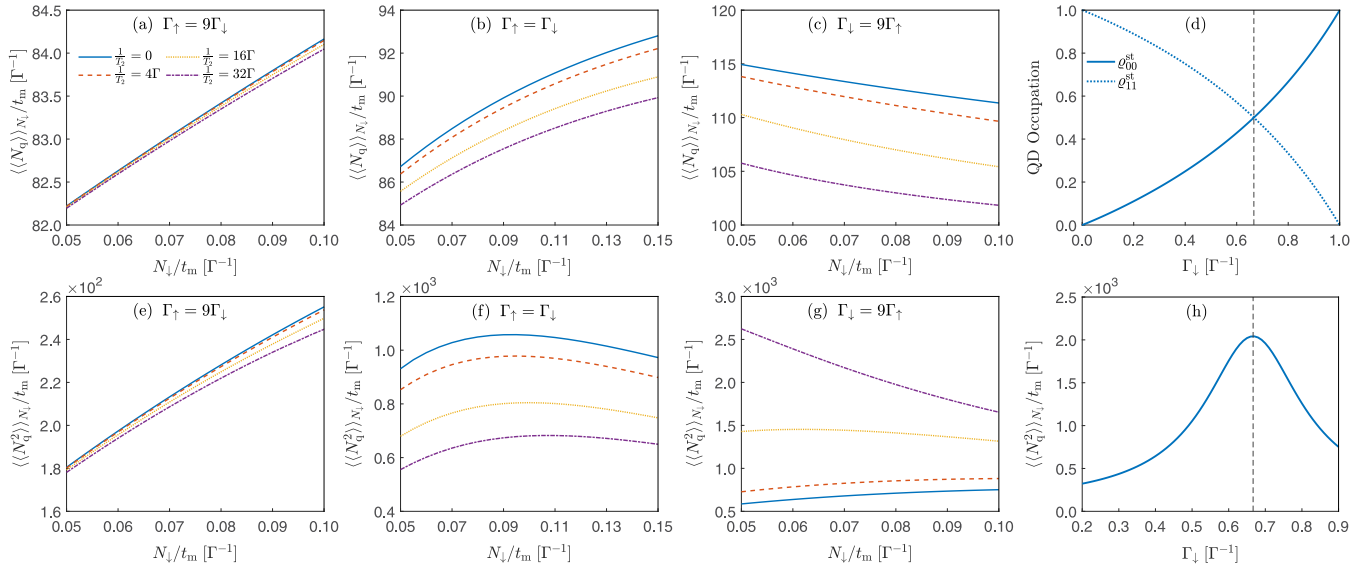

FIG. 8. Conditional QPC current for (a) $\Gamma_\uparrow = 9\Gamma_\downarrow$, (b) $\Gamma_\uparrow = \Gamma_\downarrow$, (c) $\Gamma_\downarrow = 9\Gamma_\uparrow$ and QPC noise for (e) $\Gamma_\uparrow = 9\Gamma_\downarrow$, (f) $\Gamma_\uparrow = \Gamma_\downarrow$, and (g) $\Gamma_\downarrow = 9\Gamma_\uparrow$ vs spin-resolved current $N_\downarrow/t_m$ into the QD for various environment-induced dephasing rates ($\frac{1}{T_2}$). (d) The stationary QD occupation probabilities ϱ_{00}^{st} and ϱ_{11}^{st}, and (h) the condtional QPC noise vs spin tunneling asymmetry for a spin-resolved current $N_\downarrow/t_m = 0.1\Gamma$ with $\frac{1}{T_2} \to 0$. The ESR detuning is set to zero ($\delta_{ESR} = 0$). The other plotting parameters are the same as those in Fig. 2.

through the QD. Thus, the QD is automatically implemented as a detector to investigate the conditional QPC current fluctuations without having to introduce additional amplifiers.

Figure 8 shows the influence of environment-induced dephasing on the conditional QPC current fluctuations for various spin tunneling configurations. For $\Gamma_\uparrow \gg \Gamma_\downarrow$, the QD is most of the time occupied and thus the QPC almost always exhibits the lower current I_1, except for some rare jumps due to spin tunneling events, see Fig. 1(b). If one adds an extra jump in Fig. 1(b) (see the dotted "up and down" switch), it would mean an increase in spin current and a rising of the QPC current. Both conditional QPC current and noise increase monotonically with the spin-resolved current. Furthermore, we find that both are insensitive to the environment-induced dephasing. This corresponds to the situation with minimum backaction of the QD on the QPC current cumulants.

Strikingly, for the conditional noise, anomalous dependence on the environment-induced dephasing is observed. In contrast to previous observations that dephasing increases noise [57], the condtional QPC noise is suppressed with rising dephasing rate. This unique feature is shown even more clearly for symmetric spin tunnelings ($\Gamma_\uparrow = \Gamma_\downarrow$), see Fig. 8(f).

The situation becomes very different in the opposite case of $\Gamma_\downarrow \gg \Gamma_\uparrow$, where, most of the time, the QD is empty and the corresponding QPC current is in the upper level I_0. Adding an extra jump in Fig. 1(c) (see the dotted "down and up" switch) would increase the spin current but decrease the QPC currents. This explains the results in Fig. 8(c), where $\langle\langle N_q\rangle\rangle_{N_\downarrow}$ decreases with the rising spin-resolved current. An increase in dephasing leads to incoherent spin jumps which suppress the conditional QPC current. The conditional noise shows some peculiar behavior. For weak dephasing, the conditional noise increases slightly with the spin-resolved current, see the solid and dashed curves for $\frac{1}{T_2} \to 0$ and $\frac{1}{T_2} = 4\Gamma$, respectively, in Fig. 8(g). In the case of a large dephasing rate, it decreases monotonically with spin-resolved current, see the dot-dashed curve in Fig. 8(g). This unique dependence of the conditional QPC current noise on the dephasing rate are out of the description scope of the rate equation in sequential transport through a single QD [25]. Remarkably, in contrast to the case of $\Gamma_\uparrow \gg \Gamma_\downarrow$, the conditional QPC noise now increases with rising dephasing rate.

In order to investigate the anomolous behavior and determine at which turnover point the conditional QPC noise changes its dependence on the environment-induced dephasing, we plot $\langle\langle N_q^2\rangle\rangle_{N_\downarrow}$ versus $\Gamma_\downarrow$ (with fixed $\Gamma = \Gamma_\downarrow + \Gamma_\downarrow$) for an arbitrary spin-resolved current $N_\downarrow/t_m = 0.1\Gamma$ in Fig. 8(h). We find that the turning point occurs at $\Gamma_\downarrow = 2\Gamma_\uparrow$, which corresponds to a crossing in the QD occupation [see Fig. 8(d)]. We ascribe this anomalous behavior to a combined effect of QD occupation and environment-induced dephasing. From Fig. 7(d), we observe that the QD is dominantly empty for $\Gamma_\downarrow/\Gamma_\uparrow > 2$. In this case, an increase of the dephasing leads to the loss of coherence of the system, such that the system can be described by a sequential tunneling picture. The resultant conditional QPC current noise is thus consistent with the previous observation that it increases the dephasing. In the opposite case of $\Gamma_\downarrow/\Gamma_\uparrow < 2$, the QD is most of the time occupied by an electron. A strong dephasing not only leads to the loss of coherence, but also to a prominent localization of the electron in the QD. This inhibits electron tunneling though the QD and consequently suppresses the QPC current and its noise. This reveals that the QPC current fluctuations depend sensitively on the QD occupation and environment-induced dephasing, demonstrating the great advantage of the CCS over the unconditional FCS in revealing the detailed correlation between the system and detector, even for a noninvasive detector.

V. CONCLUSIONS

We have investigated the conditional counting statistics of an ESR pumped QD coupled to a side electrode under continuously monitoring by a QPC detector. The measurement is enabled by a spin-to-charge mechanism which does not distinguish between the two spin states, such that it does not give rise to measurement-induced dephasing. In contrast to the unconditional cumulants which are independent of the QPC measurement, the detector's information backaction leads to a number of unique features in the spin-resolved conditional fluctuations and signal-to-noise ratio, which are intimately associated with the external magnetic field. We furthermore turned the perspective around and considered the QD as a "detector" to investigate the conditional QPC current fluctuations, given an observation of a spin-resolved current. We find an intriguing transition point where the conditional QPC noise changes its dependence on the environment-induced dephasing, corresponding to a crossing of the occupation of the QD. Our results unambiguously show that the information backaction of one conductor renders the statistical fluctuations of the other even for a noninvasive detector. In particular, it also implies the great potential of the conditional counting statistics to serve as a promising detection protocol in the field of quantum metrology. This work will facilitate the measurement of these intriguing correlations in near future experiments.

ACKNOWLEDGMENTS

This work is supported by the National Natural Science Foundation of China (Grants No. 11774311 and No. 12005188) and education department of Zhejiang Province (No. 8). G.E. gratefully acknowledges financial support of the Guangdong Provincial Key Laboratory (Grant No. 2019B121203002).

[1] K. Jacobs, *Quantum Measurement Theory and its Applications* (Cambridge University Press, Cambridge, 2014).
[2] H. M. Wiseman and G. J. Milburn, *Quantum Measurement and Control*, 4th ed (Cambridge University Press, Cambridge, 2010).
[3] Y. Makhlin, G. Schön, and A. Shnirman, Rev. Mod. Phys. **73**, 357 (2001).
[4] O. Gühne, E. Haapasalo, T. Kraft, J.-P. Pellonpää, and R. Uola, Rev. Mod. Phys. **95**, 011003 (2023).
[5] S. Pilgram and M. Büttiker, Phys. Rev. Lett. **89**, 200401 (2002).
[6] A. A. Clerk, S. M. Girvin, and A. D. Stone, Phys. Rev. B **67**, 165324 (2003).
[7] D. V. Averin and E. V. Sukhorukov, Phys. Rev. Lett. **95**, 126803 (2005).
[8] J. Y. Luo, H. J. Jiao, J. Hu, X.-L. He, X. L. Lang, and S.-K. Wang, Phys. Rev. B **92**, 045107 (2015).
[9] A. N. Jordan and M. Büttiker, Phys. Rev. Lett. **95**, 220401 (2005).
[10] J. Y. Luo, J. Jin, S.-K. Wang, J. Hu, Y. Huang, and X.-L. He, Phys. Rev. B **93**, 125122 (2016).
[11] S. Gustavsson, R. Leturcq, M. Studer, I. Shorubalko, T. Ihn, K. Ensslin, D. Driscoll, and A. Gossard, Surf. Sci. Rep. **64**, 191 (2009).
[12] N. Ubbelohde, C. Fricke, C. Flindt, F. Hohls, and R. J. Haug, Nat. Commun. **3**, 612 (2012).
[13] E. Kleinherbers, P. Stegmann, A. Kurzmann, M. Geller, A. Lorke, and J. König, Phys. Rev. Lett. **128**, 087701 (2022).
[14] O. Maillet, P. A. Erdman, V. Cavina, B. Bhandari, E. T. Mannila, J. T. Peltonen, A. Mari, F. Taddei, C. Jarzynski, V. Giovannetti *et al.*, Phys. Rev. Lett. **122**, 150604 (2019).
[15] D. Barker, M. Scandi, S. Lehmann, C. Thelander, K. A. Dick, M. Perarnau-Llobet, and V. F. Maisi, Phys. Rev. Lett. **128**, 040602 (2022).
[16] R. Garreis, J. D. Gerber, V. Stará, C. Tong, C. Gold, M. Röösli, K. Watanabe, T. Taniguchi, K. Ensslin, T. Ihn *et al.*, Phys. Rev. Res. **5**, 013042 (2023).
[17] *Quantum Noise in Mesoscopic Physics*, edited by Y. V. Nazarov (Kluwer Academic Publishers, Dordrecht, 2003).
[18] M. Esposito, U. Harbola, and S. Mukamel, Rev. Mod. Phys. **81**, 1665 (2009).
[19] S. Gustavsson, R. Leturcq, B. Simovic, R. Schleser, T. Ihn, P. Studerus, K. Ensslin, D. C. Driscoll, and A. C. Gossard, Phys. Rev. Lett. **96**, 076605 (2006).
[20] A. N. Korotkov, Phys. Rev. B **60**, 5737 (1999).
[21] C. A. Fuchs and R. Schack, Rev. Mod. Phys. **85**, 1693 (2013).
[22] A. Di Giovanni, M. Brunelli, and M. G. Genoni, Phys. Rev. A **103**, 022614 (2021).
[23] J. Atalaya, S. Hacohen-Gourgy, I. Siddiqi, and A. N. Korotkov, Phys. Rev. Lett. **122**, 223603 (2019).
[24] A. H. Kiilerich and K. Mølmer, Phys. Rev. A **94**, 032103 (2016).
[25] E. V. Sukhorukov, A. N. Jordan, S. Gustavsson, R. Leturcq, T. Ihn, and K. Ensslin, Nat. Phys. **3**, 243 (2007).
[26] J. Y. Luo, J. Hu, X. L. Lang, Y. Shen, X.-L. He, and H. J. Jiao, Phys. Lett. A **378**, 892 (2014).
[27] Y.-J. Chang, T.-K. Yeh, C.-H. Wan, D. W. Utami, G. J. Milburn, and H.-S. Goan, Phys. Rev. B **96**, 195440 (2017).
[28] T. Fujisawa, T. Hayashi, R. Tomita, and Y. Hirayama, Science **312**, 1634 (2006).
[29] S. A. Gurvitz, Phys. Rev. B **56**, 15215 (1997).
[30] J. Y. Luo, S.-K. Wang, X.-L. He, X.-Q. Li, and Y. J. Yan, J. Appl. Phys. **108**, 083720 (2010).
[31] H.-A. Engel, V. N. Golovach, D. Loss, L. M. K. Vandersypen, J. M. Elzerman, R. Hanson, and L. P. Kouwenhoven, Phys. Rev. Lett. **93**, 106804 (2004).
[32] S. Caprara, Nat. Mater. **15**, 1224 (2016).

[33] S. S.-L. Zhang, A. A. Burkov, I. Martin, and O. G. Heinonen, Phys. Rev. Lett. **123**, 187201 (2019).
[34] H. Bai, Y. C. Zhang, Y. J. Zhou, P. Chen, C. H. Wan, L. Han, W. X. Zhu, S. X. Liang, Y. C. Su, X. F. Han *et al.*, Phys. Rev. Lett. **130**, 216701 (2023).
[35] L. M. Gächter, R. Garreis, J. D. Gerber, M. J. Ruckriegel, C. Tong, B. Kratochwil, F. K. de Vries, A. Kurzmann, K. Watanabe, T. Taniguchi *et al.*, PRX Quantum **3**, 020343 (2022).
[36] P. M. Marcus and V. L. Moruzzi, Phys. Rev. B **38**, 6949 (1988).
[37] I. Žutić, J. Fabian, and S. Das Sarma, Rev. Mod. Phys. **76**, 323 (2004).
[38] A. N. Korotkov, Phys. Rev. B **63**, 085312 (2001).
[39] H. S. Goan, G. J. Milburn, H. M. Wiseman, and H. B. Sun, Phys. Rev. B **63**, 125326 (2001).
[40] S.-K. Wang, J. S. Jin, and X.-Q. Li, Phys. Rev. B **75**, 155304 (2007).
[41] S. A. Gurvitz and Y. S. Prager, Phys. Rev. B **53**, 15932 (1996).
[42] J. H. Shirley, Phys. Rev. **138**, B979 (1965).
[43] F. L. Traversa, M. Di Ventra, and F. Bonani, Phys. Rev. Lett. **110**, 170602 (2013).
[44] D. Dasenbrook, C. Flindt, and M. Büttiker, Phys. Rev. Lett. **112**, 146801 (2014).
[45] G. Engelhardt, S. Choudhury, and W. V. Liu, Phys. Rev. Res. **6**, 013116 (2024).
[46] Y. M. Blanter and M. Büttiker, Phys. Rep. **336**, 1 (2000).
[47] D. A. Bagrets and Y. V. Nazarov, Phys. Rev. B **67**, 085316 (2003).
[48] T. Fujisawa, Y. Tokura, and Y. Hirayama, Phys. Rev. B **63**, 081304(R) (2001).
[49] L. Cywiński, W. M. Witzel, and S. Das Sarma, Phys. Rev. Lett. **102**, 057601 (2009).
[50] H. Bluhm, S. Foletti, I. Neder, M. Rudner, D. Mahalu, V. Umansky, and A. Yacoby, Nat. Phys. **7**, 109 (2011).
[51] M. B. Lundeberg, R. Yang, J. Renard, and J. A. Folk, Phys. Rev. Lett. **110**, 156601 (2013).
[52] J. Y. Luo, Y. Yan, H. Wang, J. Hu, X.-L. He, and G. Schaller, Phys. Rev. B **101**, 125410 (2020).
[53] J. Cerrillo, M. Buser, and T. Brandes, Phys. Rev. B **94**, 214308 (2016).
[54] J. Xu, S. Wang, J. Wu, Y. Yan, J. Hu, G. Engelhardt, and J. Y. Luo, Phys. Rev. B **107**, 125113 (2023).
[55] G. Kießlich, E. Schöll, T. Brandes, F. Hohls, and R. J. Haug, Phys. Rev. Lett. **99**, 206602 (2007).
[56] J. Y. Luo, H. J. Jiao, Y. Shen, G. Cen, X.-L. He, and C. Wang, J. Phys.: Condens. Matter **23**, 145301 (2011).
[57] G. Kießlich, P. Samuelsson, A. Wacker, and E. Schöll, Phys. Rev. B **73**, 033312 (2006).